이학석사 학위논문

Micrometer-resolution Dosimetry to Study Radiosensitization of Au-Nanofilm Using Confocal Raman Spectroscopy

공촛점 라만스펙트럼을 이용한 금나노박막의 방사선량증감을 측정하기 위한 마이크론 분해능의 선량분석

2020년 02월

서울대학교 융합과학기술대학원

융합과학부 방사선융합의생명 전공

Rodrigo Hernandez Millares

A Thesis for the Degree of Master of Science

Micrometer-resolution Dosimetry to Study Radiosensitization of Au-Nanofilm Using Confocal Raman Spectroscopy

공촛점 라만스펙트럼을 이용한 금나노박막의 방사선량증감을 측정하기 위한 마이크론 분해능의 선량분석

February 2020

Program in Biomedical Radiation Sciences

Department of Transdisciplinary Studies

Graduate School of Convergence Science and Technology

Seoul National University

Rodrigo Hernandez Millares

ABSTRACT

Micrometer-resolution Dosimetry to Study Radiosensitization of Au-Nanofilm Using Confocal Raman Spectroscopy

Rodrigo Hernandez Millares
Program in Biomedical Radiation Sciences
Department of Transdisciplinary Studies
Graduate School of Convergence Science and Technology
Seoul National University

In radiotherapy, delivering accurate doses to tumors while avoiding dose deposition to healthy tissues is of great importance. The application of high Z nanoparticles to low-energy X-rays might increase this therapeutic dose window through the emission of low-energy electrons (LEE). Gold nanoparticles (GNP) present “enhanced permeation and retention” (EPR), a property in which they accumulate in the tumor vasculature. The cells surrounding the GNPs will

experience an increase in dose deposition within the subcellular range. Experimental measurement of this microscopic dose enhancement has been limited due to the lack of a dosimeter that can measure doses in a micrometer range. Currently, no experimental device can measure microscopic dose estimation within the range of the LEE emitted by GNPs. Monte Carlo (MC) simulations are the only available method to estimate the energy deposited around high Z particles. Exploring quantification of dose deposition at the micro-level with a radio chromic film appears as a promising solution. The purpose of this study is to demonstrate that confocal Raman Spectroscopy (CRS) is feasible to measure dose profile changes due to the radiosensitization of GNPs in the micrometer range on the radiochromic film.

Unlaminated radiochromic films (RCF) EBT-XD were irradiated from 0.3 to 50 Gy with a 200 kVp beam to obtain a calibration curve. The Raman spectra were obtained by positioning the post-irradiated RCF parallel to the vertical axis of the CRS microscope. The Raman peak corresponding to the C≡C diacetylene polymer stretching band was selected. The C≡C band height has proven to increase up to a saturation point due to the polymerization of diacetylene monomers. The scan resolution was set to 1 µm for a region of interest (ROI) of 100 × 5 μm^2. To investigate the radiosensitization of GNPs, another set of EBT-XD films in contact with a 100 nm gold nanofilm was irradiated at 0.5 Gy with 50 and 120 kVp beams. The dose in the active layer of the RCF was measured by averaging the C≡C peak maximum height obtained through a depth profiling from the surface to the bottom of the active layer.

The spatial resolution of the image acquisition was quantified by the modulation transfer function (MTF) method. This calculated spatial resolution implies the minimum measurable size directly. The dose deposited on the films was evaluated

in the evaluated spatial resolution. The dose enhancement factor (DEF) was obtained by comparing the doses in the films with and without gold for each measurable layer. Besides, a MC simulation for the experimental setup described above, was performed using Geant4 and compared to the experimental results. In the simulation, the dose deposition in the active layer of the RCF was measured for every 1 μm resulting in 25 segments. Furthermore, an estimation of the macroscopic DEF was made from the microscopic DEF previously obtained.

The macroscopic DEF region corresponds to the total radiochromic film volume. The macroscopic DEF was obtained by the geometric mean of the microscopic DEF measured in every layer of the RCF. Finally, for comparison, the macroscopic DEF on the film was calculated analytically using theoretical equations for dose deposition.

The experimental microscopic DEF on each segment was compared to the MC simulations, whereas the macroscopic DEF was compared amongst the experimental results, MC simulations, and analytical calculations. Together with confocal Raman spectroscopy, the radiochromic film EBT-XD obtained a spatial of ~6 μm. An experimental DEF for 50 and 120 kVp within the first 6 μm after the GNF was found to be 17.86 and 14.68, respectively and decreasing within the next layers. The macroscopic DEF for a 50 kVp beam of was 6.5, 6.8, and 5.1 for the experimental, MC, and analytical approaches, respectively. For the 120 kVp beam, macroscopic DEF of was 5.4, 5.3, 4.9, respectively.

The experimental results of the DEF obtained as a function of the distance from Au-nanofilm were consistent with data from the previous studies and our MC simulations, supporting that CRS, in conjunction with the EBT-XD system is a feasible micrometer-resolution dosimeter.

Keywords: Confocal Raman Spectroscopy, Au-nanofilm, Dose enhancement, Micrometer-resolution dosimetry, Radiochromic film, Radiosensitization.

Student Number: 2018-21685

List of Tables

List of Figures

CONTENTS

1. Introduction

Modern radiotherapy's main challenge is to deliver a cell-killing dose to tumor tissue sparing adjacent healthy tissue. Measuring the dose distribution to a micrometer scale is required in modern radiation modalities. Accurate dose measurements are necessary to ensure radiation modalities meet clinical safety standards. Current dosimeters such as ionization chambers, metal oxide semiconductor field-effect transistor (MOSFET)-based device, silicon diode detectors are specific devices for such measurements but fall short at energy dependence, tissue equivalence or micrometer range [1]. To overcome this limitation, radiochromic films have been widely employed and further studied, especially in small size dosimetry [2]. Their high spatial resolution, tissue equivalency, energy independence, and the fact that they do not require any chemical treatment for data processing and analysis, gives these films an advantage towards other dosimeters [3]. EBT-XD (Ashland Specialty Ingredients, Bridge Water Nj) is a type of radiochromic film that darkens when exposed to ionizing radiation. The active layer of the film is made of lithium salt pentacosa- 10, 12-diyonic acid (LiPCDA), a radiosensitive salt. When exposed to high energy radiation, LiPCDA monomers polymerize into a long-chained polymer whose backbone is made up of double and triple carbon bonds [4]. Usually, radiochromic films are examined through optical densitometers that measure shifts in their optical density for different doses. Recent studies have used Raman spectroscopy to determine the compositional change in the radiochromic film structure due to the polymerization of LiPCDA monomers [1-5]. Raman

spectroscopy detects the inelastic scattering of an excitation light source on a sample. The inelastic scattering, also called Raman scattering, corresponds to the vibrational states of the molecules; where only one in tenth million photons will be scattered inelastically [6]. In previous studies, Mirza et al. have proven confocal Raman spectroscopy to be feasible for micrometer dosimetry. By applying a peak ratio between the C≡C stretching band at 2058 cm^{-1} and the C-C-C deformation mode at 696 cm^{-1} the spatial resolution of the system was found to be ~3 μm [2]. With a similar experimental set up measuring only the increase on the C≡C peak, a spatial resolution of approximately 6 μm was achieved. Soares et al. mentioned that the limiting spatial resolution distinguishable in an RCF is to be considered the chromophore composing the active layer which is approximate 0.75 μm [7].

Such capability is useful for dose measurements in radiation therapy. A growing trend in radiation therapy is the application of High Z nanoparticles to low energy X-rays to increase the dose window in the vicinity of the particle due to the liberation of low energy electrons (LEE). Gold nanoparticles have become an attractive option for enhanced radiotherapy treatment due to their intrinsic properties such as biocompatibility, nonreactivity, and molecular stability. Additionally, they demonstrate a high photoelectric cross-section for low energy photon beams [8].

Furthermore, GNPs have long circulation time due to the tumor's leaky vasculature; the GNPs tend to deposit passively inside the tumor tissue. This is known as the enhanced permeability and retention (EPR) effect [9]. GNPs with a thickness smaller than 150 nm have an increased deposition in the tumor

microenvironment [10].

Jones et al. employed Monte Carlo calculations to simulate the dose deposition and dose enhancement factor on the surrounding of GNPs when irradiated with different photon energy beams. It was shown that the dose deposited due to LEE's is significantly increased within a radius of ~ 30-40 μm from the nanoparticle when irradiated by low energy beams. In a different approach, Rakowski et al. simulated a gold nanofilm (GNF) as a cluster of GNPs with a 25 nm thickness size attached to the radiochromic film EBT2, irradiated to a 50 kVp energy photon beam. A maximum microscopic DEF of 18.31 was found in the immediate region following the GNF [11]. From a clinical perspective, other studies have studied the microscopic dose distribution to estimate the cell survival fraction [12]. Mirza et al. employed different GNF sizes and energy beams to calculate the dose enhancement factor in the whole EBT-XD film using Raman spectroscopy [13].

No experimental set up has been developed able to estimate the dose enhancement at a micrometer level. Still, Raman spectroscopy and EBT-XD films have shown to have optimal characteristics for micrometer resolution dosimetry. The purpose of this dissertation is to demonstrate that confocal Raman spectroscopy, along with RCF EBT-XD is a feasible device to measure dose profile changes at a micrometer level. Measurements of microscopic and macroscopic DEF were done and compared to MC simulations and analytical calculations.

2. Material and Methods

2.A. Radiochromic films and irradiation

2.A.I Radiochromic films

EBT-XD (Ashland Specialty Ingredients, Bridge Water, Nj, Lot #12101501) film was used for this study [14]. EBT-XD technical features are explained elsewhere [15]. The film is composed of a 25 µm radiation-sensitive active layer compacted between two 125 µm PET protective layers. Figure 1.a. shows the structural diagram of an EBT-XD film. The active layer of the radiochromic film is composed of lithium salt of pentacosa-10, 12- dyonic acid monomers that are polymerized when in contact with UV-light or ionizing radiation. The polymerization reaction in the film results in a visible darkening.

The film was cut into 2 × 2 cm^2 portions. A mark was made in the upper right corner of each one of the pieces to define the film orientation. For this study, the upper PET protective layer was detached from the original structure of the film to ensure that the energy deposition by low energy radiation occurred in the active layer of the film. Figure 1.b. shows the scheme of the EBT-XD film after the PET layer detachment and collocation of the GNF in direct contact with the active layer. The films were handled with particular caution and kept at a temperature below 25^{o}C. Gloves were used throughout the whole experiment to avoid any subsequent damage made by fingerprints and to prevent dust accumulation.

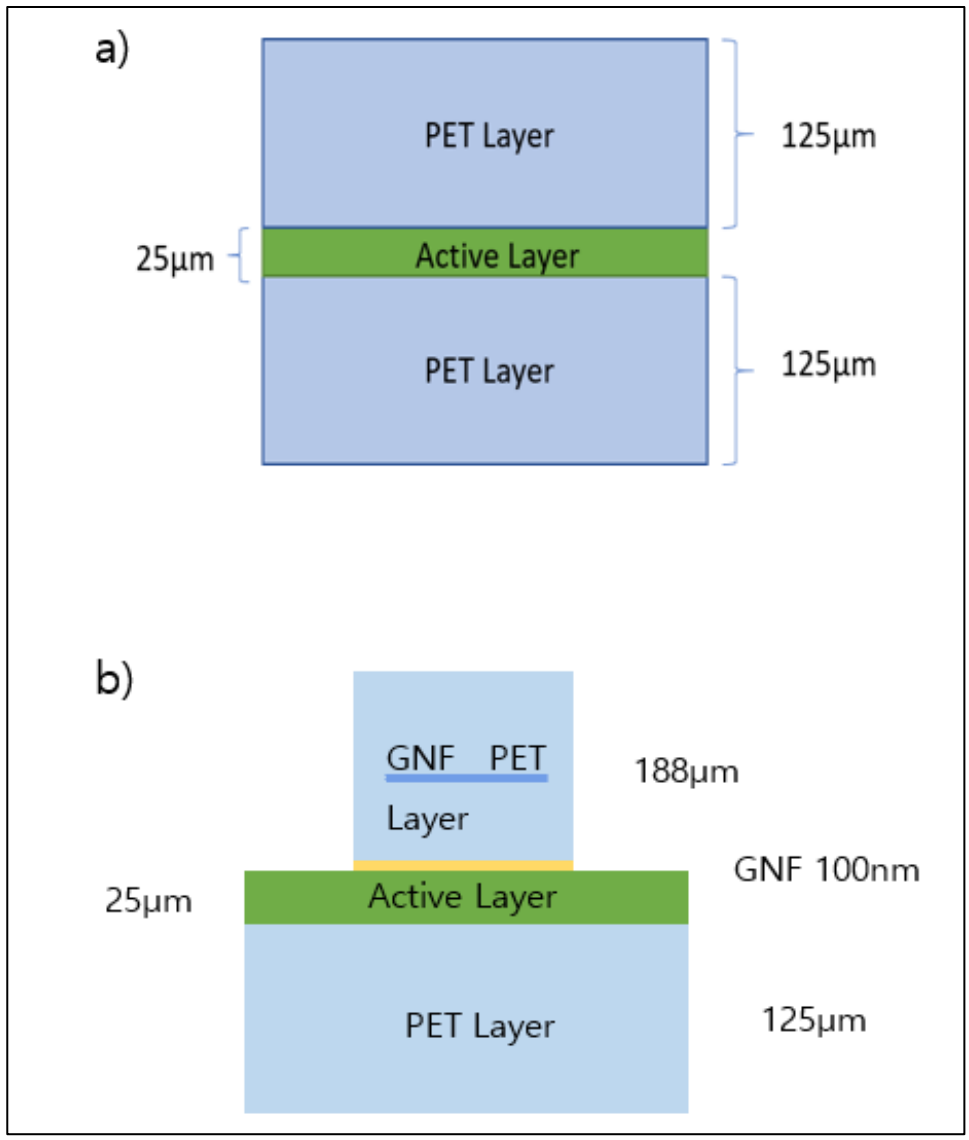

Figure 1. a) Conventional EBT-XD. The radiochromic film composed of a radiation-sensitive active layer compacted between 2 PET protective layers. b) Unlaminated EBT-XD film: To ensure the GNF was in direct contact with the active layer of the film the upper PET layer was removed

2.A.II Irradiation

EBT-XD films were irradiated with an XRAD 320 Biological Irradiator (Precesion X-Ray, Inc., N. Branford). For the calibration curve, films with no GNF attachment were delivered doses from 0.3 to 50 Gy with a source-to-surface distance of 50 cm and a field size of 10 × 10 cm^2 following the recommendations of the TG-61 [16]. The beam quality index of the 200 kVp X-rays used was 2.55-mm-thick aluminum. The films which were in direct contact with the GNF were exposed to 50 and 120 kVp X-ray beam. The delivered dose was of 0.5 Gy following the same irradiation procedure as the previous films. Figure 2 shows a diagram of the irradiation set up.

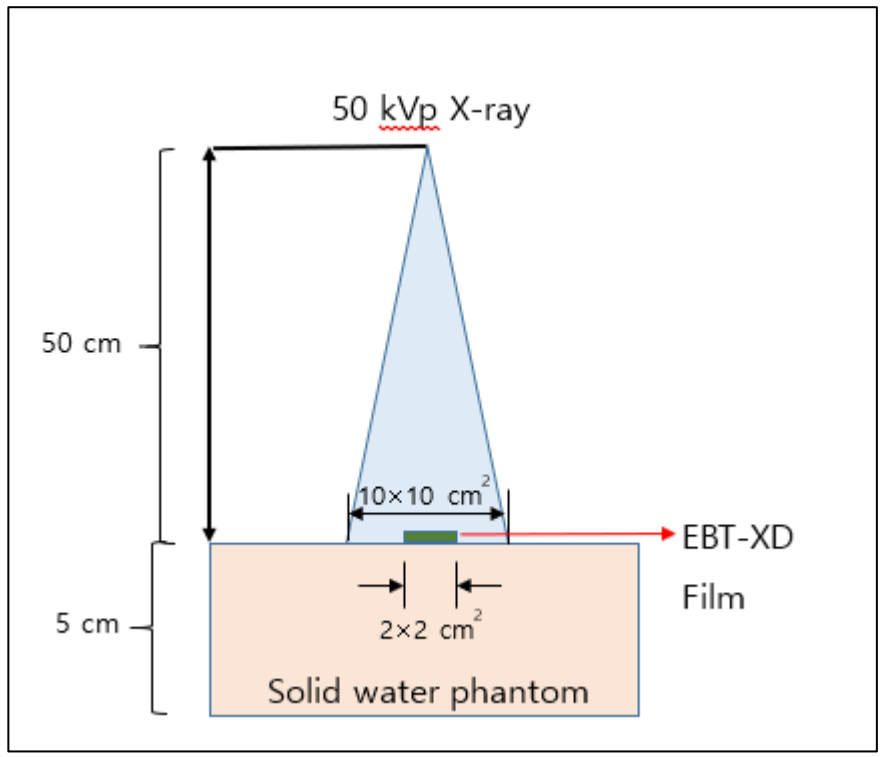

Figure 2. EBT-XD irradiation set up.

2.B. Confocal Raman micro-spectroscopy

Raman spectroscopy is a widely used technique to obtain information on the chemical composition of different samples. The Raman instrument collects the scattered light from the interaction of photons with matter. A notch filter discriminates the scattered photons of the same energy as the monochromatic excitation beam known as Raleigh scattering. The Raman scattering corresponds to the photons that experienced a loss or gain of energy due to the absorbance or release of energy by the molecule. Therefore, the scattered photon doesn't match the one of the incident lights. This effect occurs approximately in one for a million incident photons. The Raman spectrum shows a plot of the energy of the Raman scattering vs. the intensity (commonly thought as the molecular concentration), which is used for molecular identification. Each molecule will plot a unique Raman spectrum, hence often called a molecular "fingerprint" of the sample.

The microscope used to focus the laser beam onto the sample can be set confocally. The confocal system adds a pinhole on the focal plane, improving the lateral spatial resolution. The confocal system discriminates efficiently the scattered light not coming directly from the focal plane of the microscope. Figure 3 shows a basic schematic diagram of a confocal Raman spectroscopy system [6].

A confocal Raman spectroscopy system with a 30-μm pinhole was used (DONGWOO OPTRON model Ramboss-star, Korea). By utilizing a confocal system, the lateral resolution and depth profiling of a Raman scattering signal detection are significantly improved. A He-Ne red laser of 632.8 nm in combination with a dry objective U Plan SApo 100 × objective (Numerical Aperture 1.00) was used. The measurements were taken through 10 spectra accumulations with a 0.2 s laser exposure time. The grating was set to 150/300 grooves/mm resulting in smoother Raman peaks.

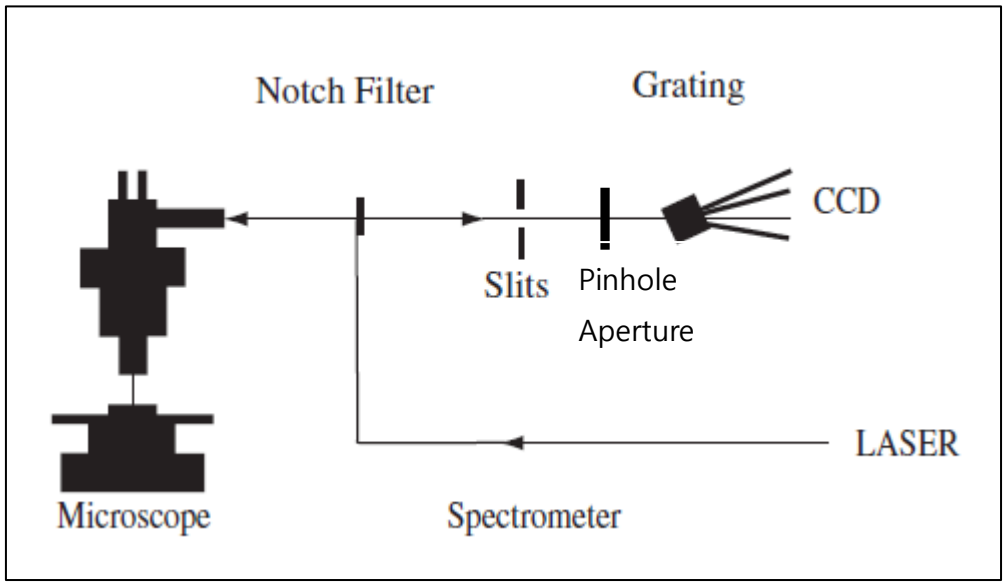

Figure 3 Basic Raman spectrometer, notch filter, spectrometer, grating, CCD detector and microscope set up confocally by the addition of a pinhole in its focal plane [6].

2.C. Raman mapping

The Raman mapping technique used for this study was set to map a region of interest (ROI) of 100 × 5 μm^2, which included a side of aluminum coating, the active layer of the film, and a portion of the PET bottom layer. The Raman spectrum of 505-pixel points was acquired for each different dose level film. Data processing included the selection of the C≡C stretching of the 505 Raman spectra. The C≡C peak intensity of the spectra was pre-processed, which included band selection, baseline removal, and fitting to a Lorentzian function. The values corresponding to the active layer of the film were averaged and plotted as a function of dose for data analysis.

2.D. Spatial resolution and active layer measurement

The spatial resolution of a microscope imaging acquisition system is defined as the minimum distance separation between two points so that they can be recognized as two different patterns [17]. The Rayleigh criterion is a commonly used criterion to define the spatial resolution of a microscope-based imaging system. The Rayleigh distance determines the spatial resolution at which two-point sources will be detected without overlapping. The equation of the Rayleigh distance will be given by

$$r_{Airy} = \delta = 0.61(\frac{\lambda}{NA})$$

Where λ refers to the wavelength of the exciting monochromatic laser, and NA is the numerical aperture of the microscope objective used. In contrast, by using a confocal system, the distance is reduced to

$$r_{Airy} = \delta = 0.43(\frac{\lambda}{NA})$$

Figure 4. shows the Rayleigh criterion for resolution. Ideally, the spatial resolution of the confocal Raman spectroscope could potentially be resolved to the pixel width (~1 μm). However, the system is limited by the amplitude of the measured signal. The amplitude of the measured signal requires to be large enough to be detected. The spatial resolution of an imaging system to a specific sample may be obtained through the Modulation transfer function (MTF) method. The limiting spatial resolution of the imaging system to the sample will be the spatial frequency at which the amplitude of the MTF decreases to 10 % modulation [18]. A plot of an MTF demonstrating the limiting spatial resolution is shown in Figure 5.

The MTF and spatial resolution of the system CRS to radiochromic film were measured by placing the RCF in an aluminum device previously manufactured. The device holds a 20 × 5 mm^2 RCF strip in a vertical position aligned to the CRS dry metallurgical objective for data acquisition as shown in Fig. 6. To avoid signal from adjacent materials, the films were coated with an aluminum tape on both laterals of the RCF. Aluminum tape was experimentally tested and proved to have no Raman signal. Figure 7. shows a schematic diagram of the RCF positioning for reading. The EBT-XD films exposed to different dose levels were placed in the central compartment of the L-shaped device. The lateral screws of the device were tightened to immobilize the RCF. The scan resolution of the CRS was set to 1 μm. Five lines of the ROI corresponding to the active layer of the film were preprocessed and fitted with an asymmetrical double sigmoidal Boltzmann function. The full width half maximum (FWHM) of the fitted function was defined as the detected active layer portion of the film. Theoretically, the spatial resolution of the RCF and CRS are both ~1 μm. To measure the approximate spatial resolution of the CRS in conjunction with the RCF irradiated with gold, the MTF was calculated. The left edge of the fitted asymmetrical double sigmoidal Boltzmann function corresponding to the gap

between aluminum (no Raman signal), and the active layer of the film, was used to calculate the edge spread function (ESF). A differential function was applied to the ESF to obtain the line spread function (LSF). The LSF was normalized to obtain the unit area. Finally, a fast Fourier transform (FFT) function was applied to the LSF, with resulting frequency and magnitude equivalent to the modulation transfer function (MTF).

The estimated spatial resolution of an imaging system is the frequency in which the MTF crosses the 10% threshold. The estimated spatial resolution of the EBT-XD film in contact with the GNF was used to establish the dose reading steps of the RCF. The C≡C band height corresponding to the useful range estimated with the spatial resolution was averaged to obtain a microscopic DEF in each portion of the active layer of the film.

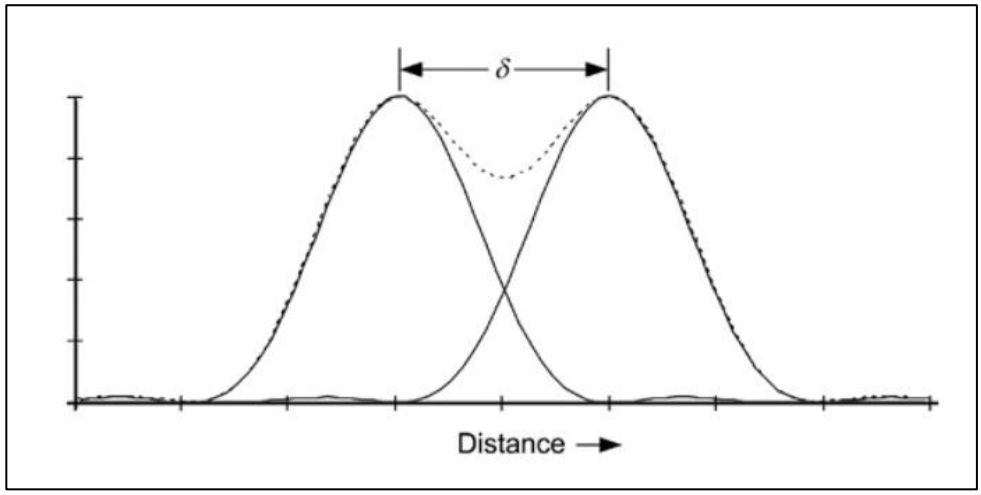

Figure 4 The Rayleigh criterion. Minimum distance resolved by two-point sources in a microscope imaging system.

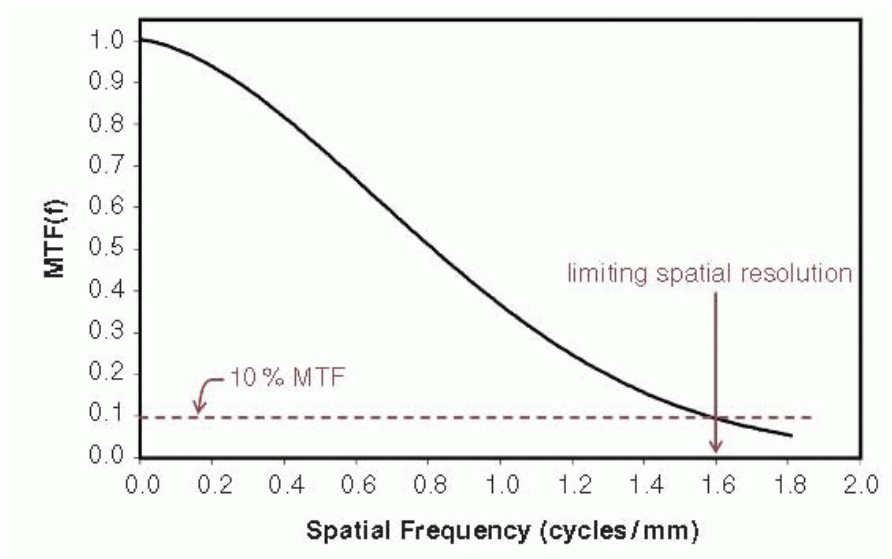

Figure 5 The limiting spatial resolution of an imaging system to a specific sample [16]

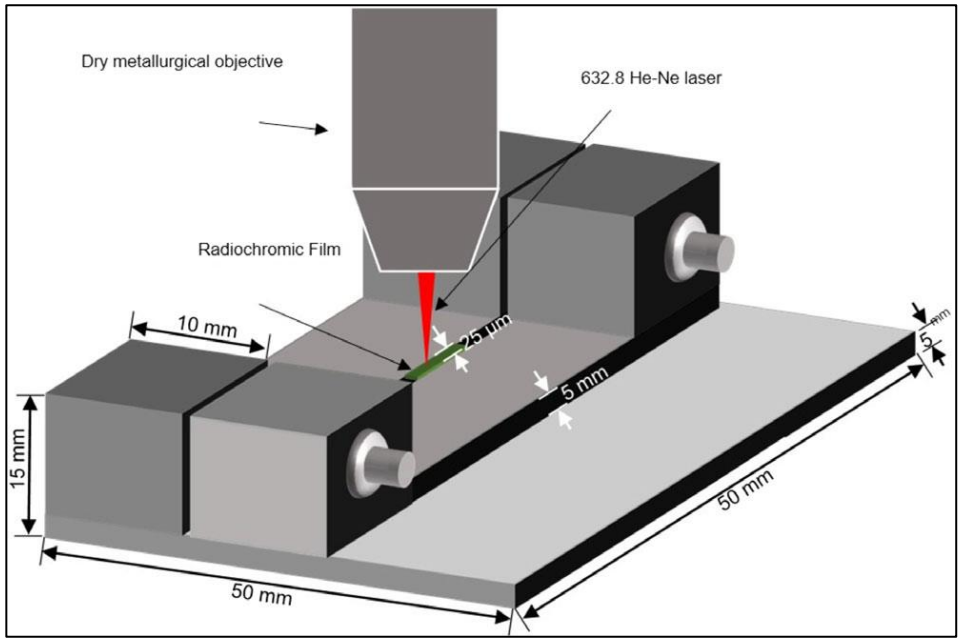

Figure 6 Manufactured device to allocate the radiochromic film in a lateral position vertical to the CRS for data acquisition. A dry metallurgical objective in conjunction with a He-Ne red laser, was used.

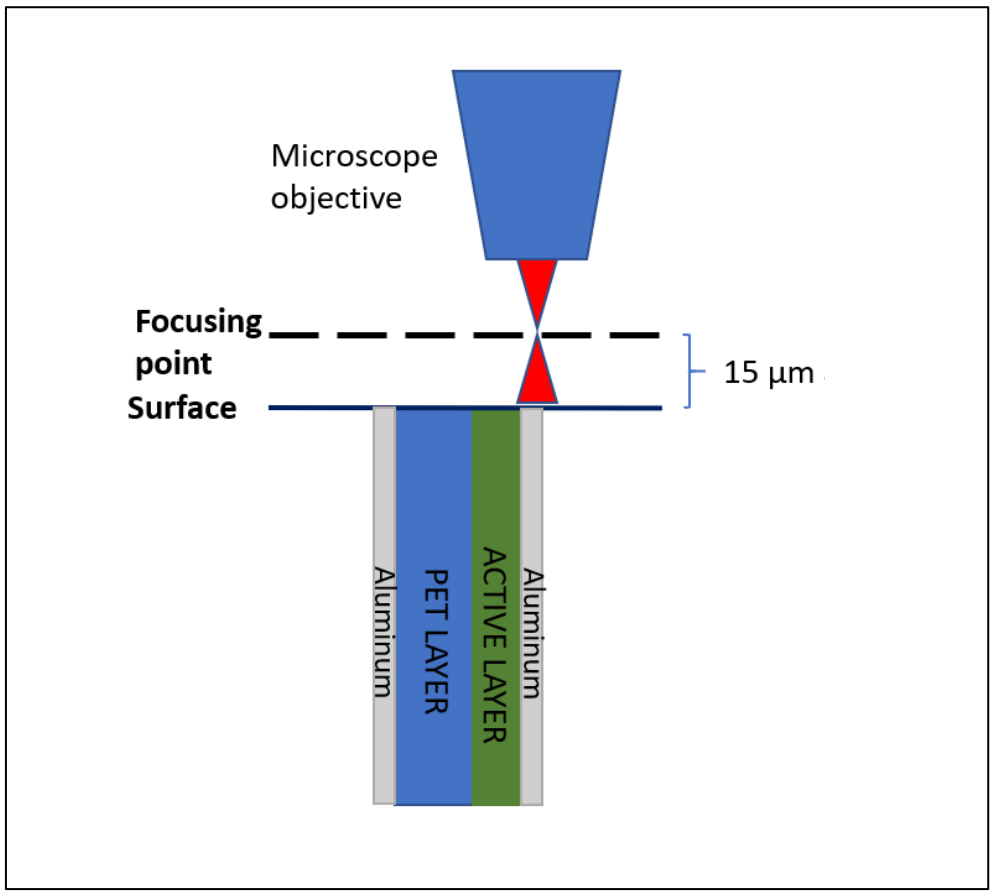

Figure 7 Schematic diagram of the RCF reading by the CRS. The film was rotated 90 degrees, and the surface of the film was positioned perpendicular to the microscope objective. Films were coated with aluminum to avoid contamination from adjacent materials. The focusing point of the laser was set 15 µm above the surface of the film.

.

2.E. Calibration curve

The FWHM of the fitted asymmetric double sigmoidal Boltzmann curve obtained from the RCF's irradiated without contact with gold was used as the range to define the active layer portion of the acquisition. The average intensity of the C≡C in the range previously defined by the FWHM in each line of the ROI was used to draw a calibration curve. The calibration curve was obtained by reading EBT-XD films exposed from 0.3Gy to 50 Gy with 200 kVp X-ray beam. A *t*-test statistical analysis was performed on all consecutive dose levels to obtain a clinically useful range.

2.F. Microscopic and Macroscopic Dose Enhancement Factor

The dose enhancement factor is defined by

$$\text{DEF} = \frac{D_{GNF}}{D_{Without\ GNF}}$$

To measure a proper DEF in the 25 μm of the film, another set of films was exposed to a 0.5 Gy dose level with beam energies of 50 kVp and 120 kVp. The GNF used for this study had a thickness of 100 nm, which was attached to the unlaminated part of the film henceforth called the surface of the active layer. The GNF was attached before irradiation and detached after completion of the radiation. A darker area in the region, which was in direct contact with the GNF, was observed. Previous Monte Carlo studies have shown that the produced LEE will deposit most of their energies within the first micrometers from gold.

The CRS objective laser would approach the side of the active layer that was uppermost during X-ray irradiation and continue in a horizontal trajectory to the bottom side of the film, as shown in Figure 7. The profiling was divided into steps of the same length as the spatial resolution previously calculated. An average of the layers was calculated from the C≡C band height and compared to the calibration curve. The corresponding dose for each slab was interpolated from the calibration curve. The ratio between the interpolated dose and the real dose (0.5 Gy) was calculated to measure the microscopic DEF in every portion of the active layer.

The macroscopic DEF defined as the dose increase in the whole active layer volume. The macroscopic DEF was obtained thorugh the geometric mean dose of the microscopic DEF, then

$$\text{Macroscopic DEF} = \left(\prod_{i=1}^{n} microscopic\ DEF \right)^{1/n}$$

Where n is the total number of layers in which the RCF was divided, and i is the initial step starting from the surface of the film.

2.G. Mont Carlo simulations

Monte Carlo simulations were carried out with the Geant 4 software. The schematic diagram of the simulation set up is shown in Figure 8. The simulation replicates completely the experimental irradiation set up. The active layer of the film was simulated according to the compositional structure shown in table 1. PENELOPE physics was employed for low energy electrons. The low energy range was set to 100 eV. Auger cascade and fluorescence were set to active. The voxel corresponding to the 25 μm of the active layer was divided into 25 sensitive detectors of 1 μm thickness each. Energy deposition scoring was made in each of the detectors. Afterward, the dose deposited in each detector of the film was calculated. A second simulation switching the GNF for a water phantom was carried out. The microscopic dose enhancement factor was calculated by obtaining the ratio between the dose deposited in each 1 μm voxels from the simulation with GNF and the simulation without the GNF. The macroscopic DEF from MC simulation was approximated by fitting a decreasing exponential curve to the obtained microscopic DEF and calculating the area under the curve.

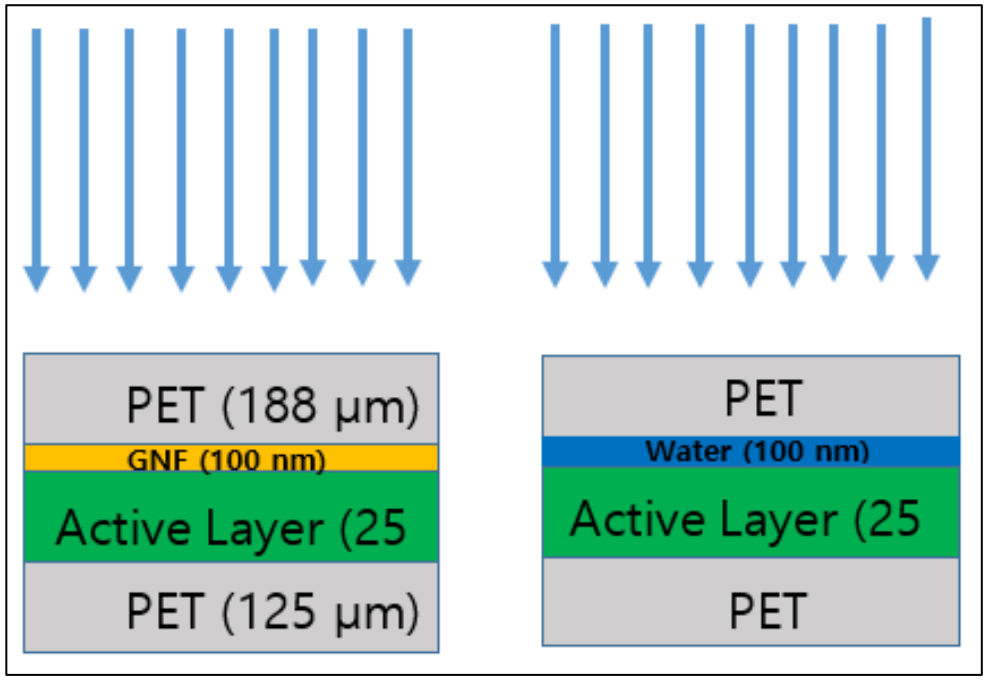

Figure 8 Monte Carlo Simulation set up. Two different simulations were carried out. Left: with a GNF attached to the active layer of the film. Right: GNF replaced with water phantom. The blue arrows represent incoming X-rays.

Table 1 Density and compositional weight of EBT-XD film used for Monte Carlo simulation and analytical calculations

Material	Density (g/cm^3)	Fractional composition weight								
		H	Li	C	N	O	S	Na	Cl	Al
PET	1.38	0.042		0.625	-	0.333	-	-	-	-
Active Layer	1.35	0.089	0.06	0.532	0.09	0.291	0.005	0.004	0.006	0.059
Protective Layer	1.35	0.042	-	0.625	-	0.333	-	-	-	-

2.H. Analytical Approach

The analytical calculations to obtain the macroscopic DEF in the RCF were calculated following a similar approach presented by Mirza et al [13].

The calculations were carried out with an X-ray energy beam of 50 kVp and 120 kVp. The thickness of the GNF used was 100 nm. A dose absorbed by the active layer of the film, not in contact with GNF by X-ray, was assumed to be 1 Gy. Under charged particle equilibrium (CPE) the absorbed dose in a medium of atomic number Z by monoenergetic photons equal to the collisional kerma [19]. The collisional kerma is defined as,

$$D_{abs} = K_c = \psi \cdot \left(\frac{\mu_{en}}{\rho}\right)_{E,Z}$$

Where ψ is the energy fluence of the photon beam, and $\left(\frac{\mu_{en}}{\rho}\right)_{E,Z}$ is the mass energy absorption coefficient of the material, dependent on the atomic number of the compound and the beam energy. The effective beam energies taken for this work of the kVp X-ray were 25.6 and 49.5 keV for 50 kVp and 120 kVp respectively [19]. The energy fluence was calculated by multiplying the photon fluence Φ, times the effective energy. The value of the mass-energy absorption coefficient of any compound can be calculated by knowing the fractional composition of each element in the sample as,

$$\left(\frac{\mu_{en}}{\rho}\right)_{E,Z} = f_{Z1}\left(\frac{\mu_{en}}{\rho}\right)_{E,Z1} + f_{Z2}\left(\frac{\mu_{en}}{\rho}\right)_{E,Z2} + f_{Z2}\left(\frac{\mu_{en}}{\rho}\right)_{E,Z3} + \cdots$$

The fractional composition to calculate the mass-energy absorption coefficient of the EBT-XD was taken as per table 1.

To calculate the DEF in the active layer of the film, three different dose sources from the interaction of photons with gold were assumed: Dose from photoelectrons, dose from Auger electrons, and dose from fluorescence. These three dose sources can be obtained by,

$$D_{PE} = \Phi_{PE} \times \frac{T_0 \cdot [1 - Y(T_0)]}{\rho \cdot t}$$

Where Φ_{PE} is the photoelectron fluence, T_0 is the average energy of the photoelectrons, ρ, and *t* are the density and thickness of the active layer, respectively.

$$D_{AE} = Y_{AE} \times \Phi_{PE} \times \frac{T_{ex}}{\rho \cdot t}$$

Where Y_{AE} is the Auger electron yield from the interaction of photons with gold, and T_{ex} is the residual kinetic energy of the Auger electrons that reach the active layer, knowing that part of the generated auger electrons will deposit their energy inside the gold fold.

$$D_{Fl} = Y_{Fl} \times \Phi_{PE} \times (P_X \cdot Y_L \times E_{bX}) \times \left(\frac{\mu_{en}}{\rho}\right)_{PL \times EbL1,RCF}$$

Where P_X is the fraction of photoelectric interactions in X subshell, Y_L is the fluorescence yield of in X shell, and E_{bX} is the binding energy of the X shell. For the fluorescence yield, the mass-energy absorption coefficient to the fluorescence photons energy was used.

The dose deposited by LEE generated in the gold fold that reaches the active layer of the film is given by,

$$D_{Au} = (D_{PE} + D_{AE}) \times f_{fwd} + 0.5 D_{Fl}$$

Where f_{fwd} is the fraction of photo and Auger electrons emitted in the gold film that head to the active layer of the EBT-XD. Since the fluorescence X-ray are assumed to be emitted isotopically, only 70% are expected to direct to the EBT-XD.

Knowing the dose imparted by the different physical interactions of photons with gold, the macroscopic DEF is

$$DEF = 1 + D_{Au}$$

Assuming a dose absorbed by the film without the gold fold of 1 Gy.

3. Results

3.A. Thickness measurement and calibration curve

The color maps corresponding to the C≡C maximum height of an ROI of 100 × 5 µm for the dose levels of 0.5 to 4 are presented in figure 9.a. Color maps were obtained through all dose levels up to 50 Gy. The blue area represents part of the device which has no Raman signal attributed to the aluminum coating of the film. In contrast, the red part corresponds to the signal detected due to the C≡C stretching band.

The fitted curve of the depth profile from the doses from 0.5 Gy to 4 Gy are shown in figure 9.b. The curve fitting was made in all the dose levels. The FWHM of the fitted curve was considered as the experimental value for the thickness of the active layer of the film. The theoretical value given by the EBT-XD specifications is 25 µm. Table 2. presents the FWHM obtained from all the RCF analyzed irradiated with doses from 0.3 up to 50 Gy. Also, the mean value of the C≡C Raman intensity corresponding to the active layer of the film region for each dose level is shown in table 2.

The mean values of the C≡C band heights in the range perceived as the active layer of the film at different dose values are presented in figure 10. The error bars indicate one standard deviation from the mean. Each black square represents the mean value for a single dose level. The experimental values were fitted to an exponential curve shown as a continuous red line. The clinical dose range of the EBT- XD RCF was found up to 15 Gy.

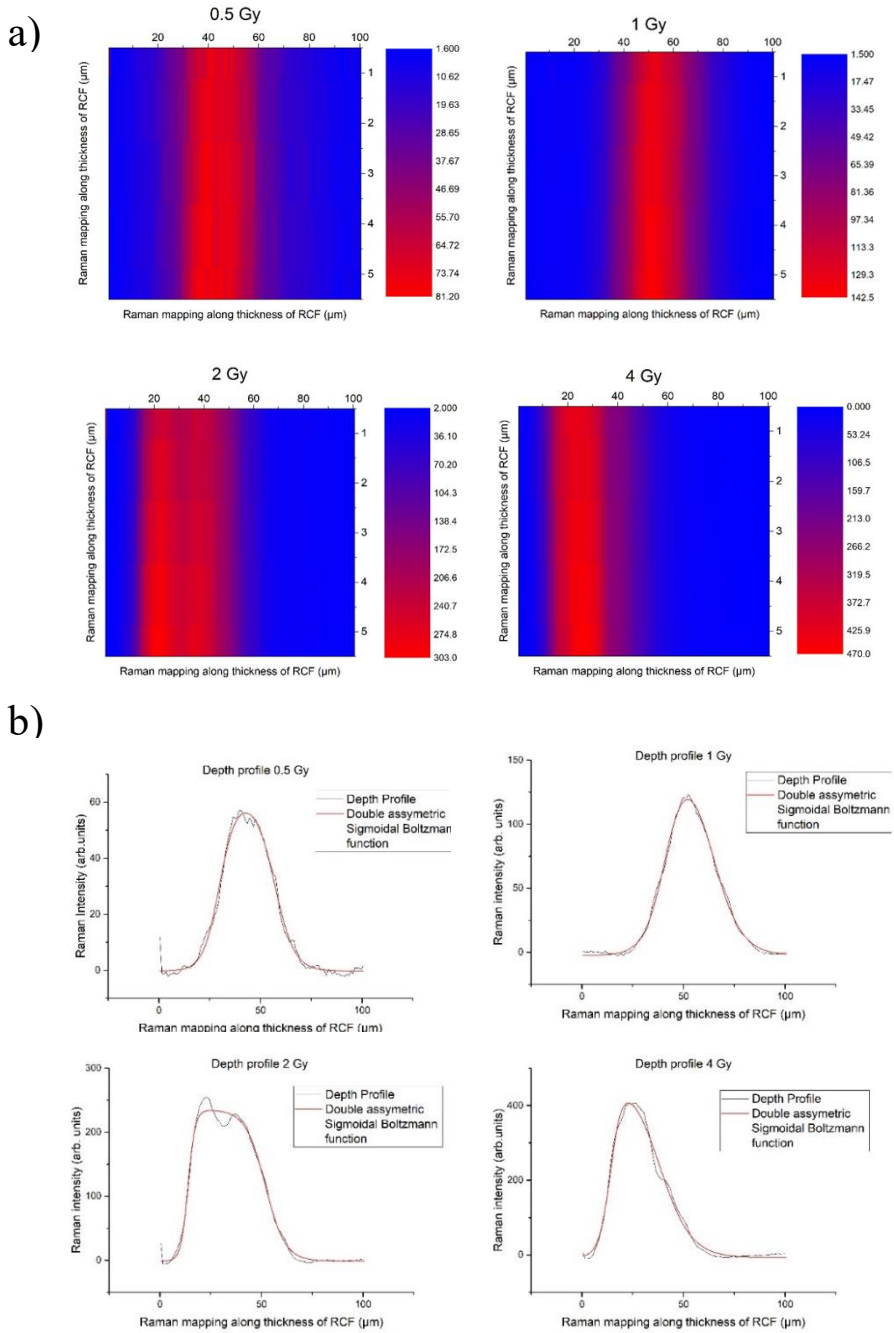

Figure 9 a) Color maps of 100 × 5 µm ROI where the color level corresponds to the C≡C band height. Each column was averaged to obtain a depth profile. b) Raman intensity profiling fitted to a double asymmetric Sigmoidal Boltzmann function to get the FWHM.

Table 2 FWHM obtained from the double asymmetric double sigmoidal curve. The FWHM was used as the experimental thickness of the active layer of the film. Averaged value of the Raman intensity of the film within the range of the measured active layer of the film in the dose levels from 0.5 to 50 Gy.

Dose [Gy]	FWHM [μm]	Mean [arb. Units]	RSD [%]
0.3	39.7	51.69	11.74308
0.5	28.66	66.64	12.48499
1	28.56	110.14	18.63083
2	38.67	249.66	14.28743
4	33.57	352.54	19.15244
8	23.06	575.89	28.94476
10	33.35	582.5	17.78026
15	25.22	657.33	17.81601
30	25.81	648.68	21.59308
50	14.06	731.36	17.8339

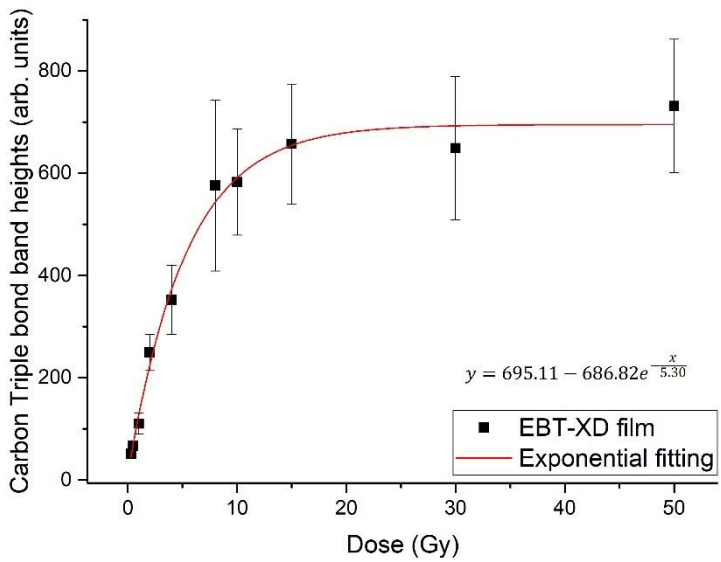

Figure 10 Dose calibration curve with Raman intensity of carbon triple bond from 0.3 to 50 Gy. The Raman intensities were fitted to an exponential function with an R-squared value of 0.9998, which is shown as a continuous red line.

3.B. Spatial resolution of GNF to RCF

Figure 11.a shows the color map corresponding to Raman intensity of the C≡C band height of the RCF attached to a 100 nm GNF exposed to 50 kVp x-rays over the 100 × 5 μm ROI. The corresponding depth profile is shown as an upper plot of the figure. Figure 10.b. shows a similar color map and depth profile of an RCF in direct contact with a GNF exposed to 120 kVp X-rays. The left sides of the depth profiles shown in figure 12 were used as the ESF. Figure 12. a. shows the MTF obtained from the ESF of the profile from the 50 kVp irradiated film. The spatial resolution estimated through the MTF method was 0.14 cycles/μm, which is ~ 6 μm. Figure 12 b. similarly presents the MTF of the film exposed to 120 kVp, which estimated a spatial resolution of ~ 6 μm.

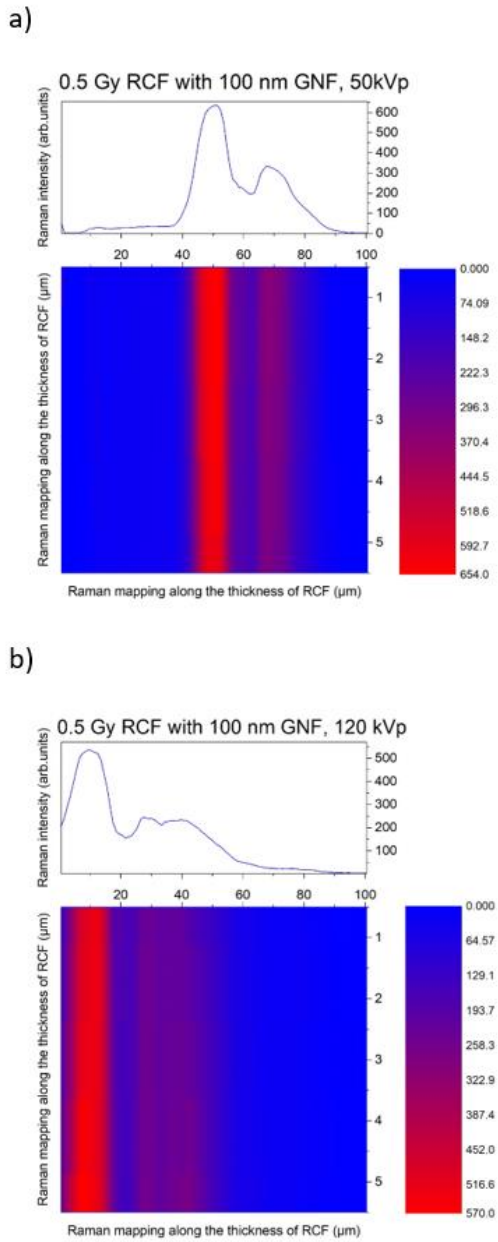

Figure 11 a) Color maps of a 100 × 5 μm ROI where the color level corresponds to the C≡C band height of RCF attached with GNF exposed to 50 kVp X-rays. b) Exposed to120 kVp X-rays. On the upper part of each appears the plot of the depth profile as an average of each column.

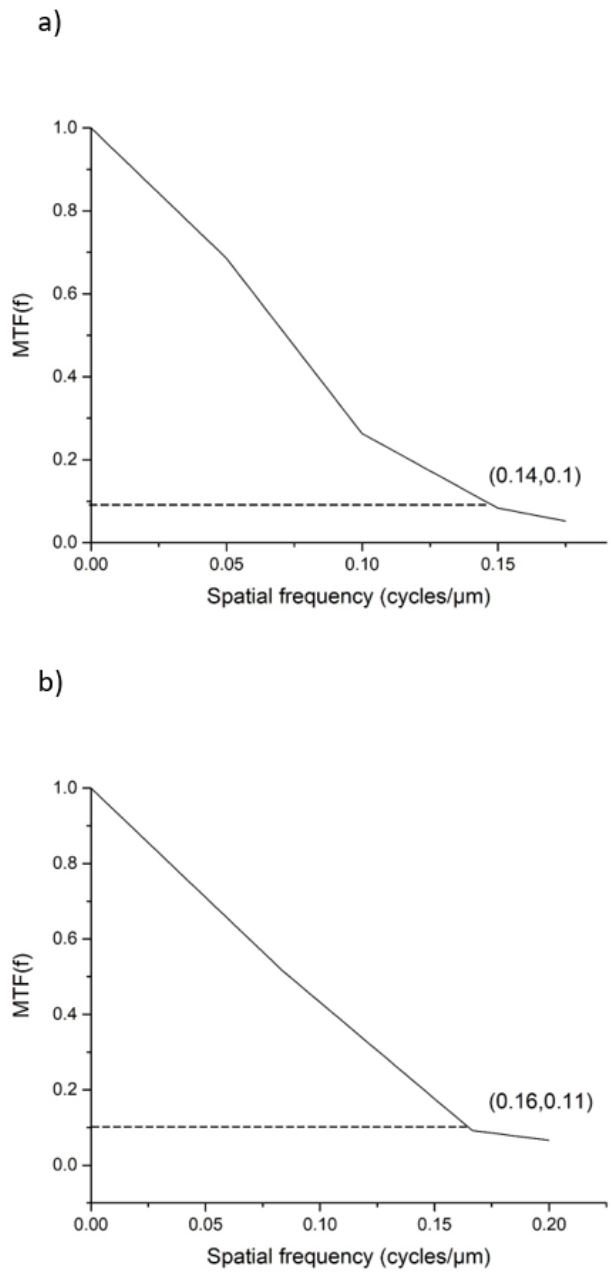

Figure 12. a) Modulation transfer function obtained from the left ESF of the RCF with GNF irradiated to 50 kVp X-rays. b) Exposed to 120 kVp X-rays.

3.C. Microscopic DEF

The microscopic DEF was obtained for two different X-ray energies of 50 kVp and 120 kVp. Figure 13. shows the microscopic dose enhancement factor estimated by MC simulation in every 1 µm of the active layer. Table 3. presents the DEF estimated per µm as a function of distance from GNF. A high dose increase is observed in the first microns of the side that was attached to the GNF. The 50 kVp X-ray shows a DEF of 60.09 in the first micron. In contrast, the 120 kVp beam shows a 30.20 increase in dose deposition at 1 micron after GNF.

The experimental value of the microscopic DEF was calculated by obtaining the mean value in every 6 µm of the irradiated RCF attached to the GNF, as the spatial resolution dictates the minimum detectable range by the CRS to RCF system. Four different values of DEF were obtained from the surface layer of the film to the bottom of it, completing the 25 µm of the active layer. To measure the microscopic DEF of every 6 um with the MC simulation, the MC estimated DEF was fitted to an exponential decay curve, and the area under the curve for every 6 µm was used for comparison against experimental results. The R-squared values from the exponential fittings of the 50 kVp and 120 kVp were 0.9993 and 0.9996, respectively. Figure 14 a. and b. show the comparison of the microscopic DEF obtained through MC simulation to the one calculated experimentally for the different energy beams studied. It is worth noting how the experimental microscopic DEF follows the same trend of the MC simulation but unlike the simulation the experimental DEF doesn't reach unity. The experimental DEF in the first 6 µm was 17.87 and 14.68 for the 50 kVp and 120 kVp beam, respectively.

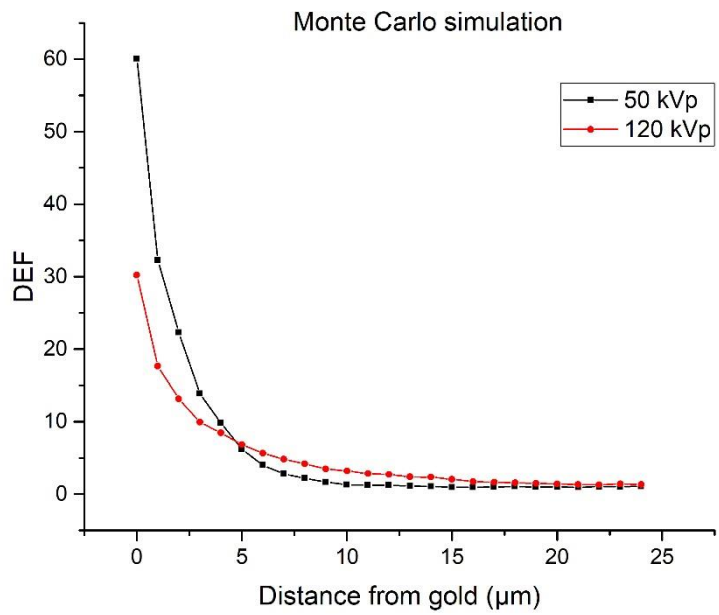

Figure 13. Microscopic DEF on every 1 μm of the active layer of the EBT-XD obtained from Monte Carlo simulation. The black squares correspond to the DEF when a 50 kVp beam irradiates gold, whereas the red circle represents the DEF values by a 120 kVp.

Table 3 Values of microscopic DEF by Monte Carlo simulation for every 1 micron scoring inside the active layer of the EBT-XD film. The DEF was measured as distance from gold.

Monte Carlo Simulation		
RCF distance from gold	DEF 50kVp	DEF 120 kVp
0	60.09	30.20
1	32.25	17.66
2	22.32	13.13
3	13.89	9.92
4	9.83	8.46
5	6.19	6.83
6	4.00	5.65
7	2.80	4.82
8	2.20	4.18
9	1.67	3.48
10	1.30	3.21
11	1.24	2.82
12	1.24	2.73
13	1.11	2.40
14	1.08	2.34
15	0.95	2.06
16	0.97	1.73
17	0.98	1.66
18	1.06	1.58
19	0.98	1.49
20	1.00	1.40
21	0.95	1.34
22	1.04	1.29
23	1.04	1.39
24	1.06	1.34

a)

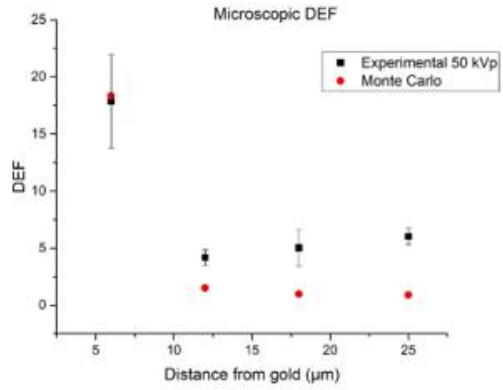

b)

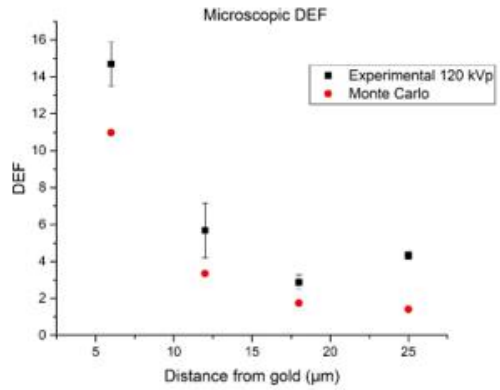

Figure 14 a) Comparison between the microscopic DEF obtained in every 6 µm step size of the radio chromic film by Experimental procedure and MC simulations when irradiated by a 50 kVp X-rays. b) when irradiated by a 120n kVp X-rays. The black square represents the experimental values and the red circles the MC values.

.

Table 4 DEF obtained for every 6-layer size range on the active layer of the film for the experimental procedure.

RCF range [μm]	Experimental DEF 50 kVp	SD	MC 50 kVp	Experimental DEF 120 kVp	SD	MC 120 kVp
0-6	17.87	4.08	18.33	14.68	1.21	10.98
7-12	4.18	0.66	1.52	5.68	1.48	3.35
13-18	5.02	1.58	0.98	2.88	0.39	1.75
19-24	6.03	0.69	0.90	4.32	0.20	1.41

3.D. Macroscopic DEF

The macroscopic DEF in the EBT-XD film was calculated via experimental, MC simulation, and analytical calculations. Figure 15. shows the comparison between the three methods employed for this study. In addition, table 5 summarizes the macroscopic DEF obtained by each one of the methods employed. Note how the macroscopic DEF in the complete EBT-XD film is reduced by increasing the beam energy. Also, the 50 kVp results for the three modalities show a higher deviation than to the ones obtained from the 120 kVp. The macroscopic DEF obtained for the 50 kVp beam was 6.52, 6.84, and 5.19 for the Raman procedure, MC simulation, and analytical calculations, respectively. For the case of the 120 kVp, a resulting macroscopic DEF of 5.43, 5.42, and 4.98 was obtained. In both energy beams studied, the estimated DEF from the MC simulation and the analytical calculations lie inside one standard deviation of the experimental values.

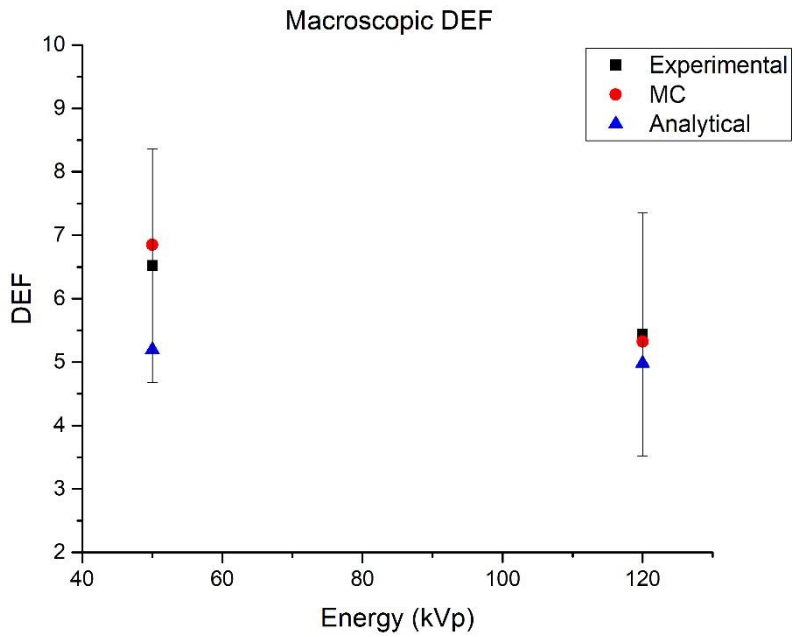

Figure 15 Macroscopic DEF obtained from the three different methods used in this study. The black square corresponds to the experimental value, the red circle to the MC simulation and the blue triangle to the analytical calculations. The error bar corresponds to one standard deviation from the experimental result.

Table 3. Macroscopic DEF measured by Raman spectroscopy, Monte Carlo simulations and theoretical calculations.

Macroscopic DEF				
Beam energy	Experimental DEF	SD	MC	Analytical
50 kVp	6.52	1.83	6.84	5.19
120 kVp	5.43	1.92	5.32	4.98

4. Discussion

The minimum point source signal that can be detected by both the CRS and the EBT-XD film is ~1 μm, as reported by the Rayleigh criterion and the size of the chromophores in the active layer of the film. As reported by Mirza et al., it was possible to achieve a spatial resolution of the CRS and RCF system of approximately 6μm measuring only the C≡C band height [2].

Table 2. presents the FWHM obtained after fitting a double asymmetrical double Sigmoidal function. The real value, as presented by the specifications of the EBT-XD is 25 μm. The FHWM derived experimentally for all the dose levels range from 14-40 μm, having a similar value as the correct value.

Previous studies have been trying to measure the dose deposition by the LEE around the GNP of different sizes [10,11,20]. Figure 13. shows the microscopic dose enhancement factor obtained from the CRS experimentation and MC simulation with geant4. It is shown how a GNF irradiated with X-rays will emit a high number of electrons, which will deposit their energy within a small range from the GNF. The GNF, when exposed to X-rays, will emit Auger and photoelectrons, which range won't surpass the 4 μm, whereas the 120 kVp will emit a higher range photoelectron reaching as long as 20 μm [13]. Sung et al. simulated the Auger electrons emission when a GNPs with diameters from 5 to 50, which were coated with different radio-isotopes. The results showed most of the Auger electrons would slow down and deposit their energy in a nm radial distance within the first μm [21]. The Auger electron's contribution to the increase in dose will be observed in the subsequent nm

after the GNF. The most significant contribution to the DEF will be given by the photoelectrons, whose energy deposition will extend a few micrometers. It can be seen in Figure 14 how the 50 kVp DEF is higher within the first microns but experiencing a fast drop to 1; on the other hand, the 120 kVp beam with a higher range of photoelectrons experience a slower decrease, which extended to ~17 μm. The microscopic DEF found within the first 6 μm of the active layer for the 50 and 120 kVp was 17.87 and 14.68, respectively. Regulla et al. also used a 150 μm thickness gold film to measure a physical DEF with a thermally simulated exoelectron emission detector, which resulted in 100 DEF within a 10 micrometers range when irritated with a 40 kVp x-rays [22]. Rakowski et al. performed a similar simulation with a 20 nm gold fold attached to an EBT2 film irradiated with the same energy beams to obtain a microscopic DEF in the surroundings of a GNF and demonstrated an 18.31 dose deposition in the RCF [11]. The experimental results measured in this dissertation are comparable to previous studies measuring the DEF induced by a GNF in a micrometer scale.

The experimental results show an increase in the DEF over the last μm of the active layer. The bottom part of the RCF is attached to a PET layer, and the focusing point of the CRS was set to 15 μm above the surface of the film. While the excitation beam approaches the PET layer, more of it will be illuminated and will scatter Raman rays to the detector. Any scattered photon that passes through the focal point will pass through the confocal aperture and be detected, contaminating the last micrometers spectra from the RCF [23]. The application of immersion oil to the sample may reduce the environmental conditions observed. In addition, Oliver et al.

demonstrated a high microdosimetric spread of the deposited dose when measuring volumes of a few microns, which explains the high deviations shown for the 50 kVp irradiation [24].

The Analytical approach underestimated the results obtained experimentally and by MC simulation. Roeske et al. stated that the underestimation of analytical calculations might be attributed to the not inclusion of secondary processes and photons produced by the interaction of primary photons [25].

The macroscopic dose enhancement factors obtained through the three different methodologies within this study are shown in figure 13. The macroscopic DEF found for 50 kVp X-rays with experimental, MC simulation, and analytical calculations were 6.52, 6.84, and 5.19, respectively. Whereas for the 120 kVp, the macroscopic DEF were 5.43, 5.32, and 4.98, respectively. The experimental results showed similarities with the MC simulation, and with the analytical approach. All three methodologies employed to calculate the macroscopic DEF agree with previous studies of DEF made on RCF's [13]. The elevated values of the experimental results towards the end of the active layer are attributed to the contamination of the last microns due to the attached pet layer.

The experimental results obtained within this work showed a similar trend as described by previous MC studies. In a micrometer scale, the experimental results and MC simulations overlap within the first 6 micron, but towards the bottom of the film, the inclusion of unwanted signals limits the scope of this study. Drawbacks of this work are the out of focus signals from adjacent materials that contaminate the

final reading by the spectroscope. Also, the physical characteristics of a GNF may differ from those of a gold nanoparticle, as they present self-absorption.

5. Conclusions

The Raman signal of the C≡C stretching band was able to detect different dose deposition within a few micrometers in the active layer of the film. MC simulations and analytical calculations were carried to compare with the results obtained experimentally, which supported the feasibility of confocal Raman spectroscopy for micrometer level resolution dosimetry. It was possible to experimentally measure the radio enhancement induced by LEE's in 6 µm steps, which to the knowledge of the author it's the first experimental dosimeter system to detect radio sensitization in the micrometer scale. The results shown indicate the enormous potential of confocal Raman spectroscopy in dosimetry. The scope of the applications of Raman spectroscopy as a dosimeter might be broadened due to the achievable high spatial resolution described in this work.

REFERENCES

1. O.S. Talarico, T.A. Krylova, N.N. Melnik, "Raman Scattering for dosimetry using GAFCHROMIC EBT3 radiochromic dosimetry film," Med.Phys. 46, 1883-1887, (2019).
2. J.A. Mirza, R. Hernandez, G.I. Kim, S-Y. Park, J. Lee, S-J. Ye, „Characterization of radiochromic films as a micrometer-resolution dosimeter by confocal Raman spectroscopy,“ Med.Phys. 46,5238-5248, (2019).
3. E.Y. Leon-Marroquin, D.J. Mulrow, R.Kahn, A. Darafsheh, "Spectral analysis of the EBT3 radiochromic films for clinical photon and electron beams," Med.Phys. 46, 973-982(2019).
4. M. Callens, W. Crijins, V. Simons, I. De Wolf, T. Depuydt, F. Maes, K. Haustermans, J.D'hooge, E.D'Agostino, M.Wevers, H.Pfeiffer, K. Van Den Abeele, "A spectroscopic study of the chromatic properties of GafChromic ™EBT3 films," 43, 1156-1166 (2016).
5. J.A Mirza, H. Park. S-Y. Park, S-J, Ye, „Use of radiochromic film as a high spatial resolution dosimeter by Raman spectroscopy,“ Med.Phys.43,4520-4528(2016).
6 E. Smith and G. Dent, Modern Raman spectroscopy-A practical approach (John Wiley & sons LTD., England, 2005)
7. C.G Soares, "Radiochromic film dosimetry," J. Rad. Meas. 41, S100-S116 (2007).
8 B,L Jones, S. Krishnan, S.H. Cho, "Estimation of microscopic dose enchancement factors around gold nanoparticles by Monte Carlo calculations," Med. Phys. 37, 3809-3815.
9. H. Kobayashi, R. Watanabe, P.L. Choyke, "Improving conventional enhanced permeability and retention (EPR) effects; What is the appropiate target," Theranostics, 4, 81-89 (2014).
10. L. A Bennie, H. O. McCarthy, J. A. Coulter, "Enhanced nanoparticle delivery exploiting tumour-responsive formulations," Cancer Nanotechnology, 9 (2018)
11. J.T. Rakowski, S.S. Laha, M.G. Snyder, M. G. Buczek, M. A. Tucker, F.L Liu, G. Mao, Y. Hillman, G. Lawes, "Measurement of gold nanofilm dose enhancement using unlaminated radiochromic film," Med. Phys. 42, 5937-5944 (2015).
12. Y. Lin, S. J. McMahon, H. Paganetti, J. Schuemann, "Biological modeling of gold nanoparticle enhanced radiotherapyfor proton therapy," Phys. Med. Biol. 60, 4149-4168 (2015)
13. J.A. Mirza, K. Choi, W. Sung, S. Jung, S-J. Ye, "Measuring radioenhancement by gold nanofilms: Comparison with analytical calculations," Physica Medica. 68, 1-9 (2019).
14. Ashland Specialty Ingredients, 1005 US Highway 202/206, Bridgewater, NJ 08807.
15. Gafchromic™ EBT-XD film specifications, available at http://www.gafchromic.com
16. C-M. Ma, CW. Coffey, LA. DeWerd, et al. AAPM, protocol for 40-300 kV x-ray beam dosimetry in radiotherapy anmd radiobiology. Med. Phys. 28,863-893(2011).
17. K.R. Castleman, F. Merchant and W. Qiang, Microscope Image Processing, (Elsevier Inc, 2008)
18 J.T. Bushberg, J.A Seibert, E.M Leidholdt, J.M Boone, The esstial physics of Medical Imaging. Philadelphia, PA: Lippincont Williams & Wilkins. 2012; 39-41.
19. F.H. Attix, "Introduction to radiological physics and radiation dosimetry. Wiley-VCH Verlag GmbH & Co. KGaA, Weinheim 2008.

20 M. Hamdi, M. Mimi, M. Bentourkia, "Comparison between X-ray spectra and their effective energies in small animal CT tomographic imaging and dosimetry," Australias Phys. Eng. Sci. Med, 40 20-37 (2017).

21 W. Sung, S. Jung, S-J. Ye, "Evaluation of the microscopic dose enhancement for nanoparticle-enhanced Auger therapy," Physics in Medicine and Biology. 61, 7522-7535(2016).

22 D.F. Regulla, L.B. Hieber, M. Seidenbusch, "Physical and biological interface dose effects in tissue due to X-ray-induced release of secondary radiation from metallic gold surfaces," Radiat.Res. 150, 92-100 (1998).

23 N. Everall, "The Influence of Ou-of-Focus Sample Regions on the Surface Specificity of Confocal Raman Spectroscopy," Applied Spectroscopy. 62, 591-598(2008).

24. P. A.K. Oliver, M. Thomson, "Microdosimetric considerations for radiation response studies using Raman spectroscopy," Med. Phys. 45. 4734-4743 (2018).

25. J. C. Roeske, L. Nuñez, M. Hoggarth, E. Labay, R. R. Weichselbaum, "Characterization of the theoretical radiation dose enhancement from nanoparticles," Technol. Canc. Res. Treat. 6, 395-401 (2007).

Abstract (in Korean)

국 문 초 록

방사선 치료에서 건강한 조직에 대한 선량 축적을 피하면서 종양에 정확한 선량을 전달하는 것은 매우 중요하다. 저 에너지 X 선에 높은 원자번호의 나노 입자를 적용하면 저 에너지 전자(low energy electron, LEE)의 방출을 통해 방사선 치료용 선량 창을 늘릴 수 있다. 금 나노 입자(gold nano-particle, GNP)는 종양 혈관 속에 축적되는 특성인 "투과 및 보존 강화"(enhanced permeation and retention, EPR)를 가지고 있다. 금 나노 입자를 둘러싼 조직은 세포 이하의 범위 내에서 전달 선량이 증가하는 효과를 받을 것으로 기대된다. 마이크론 범위에서 측정할 수 있는 선량 측정법의 부재로 미시적 선량 향상에 대한 실험적 측정이 제한되었다. 지금까지는 어떤 장치도 GNP 가 방출하는 LEE 범위 내에서 미시적 선량 추정치를 측정할 수 없었다. 몬테카를로 시뮬레이션만이 높은 원자번호의 입자 주변에 축적되는 에너지를 측정할 수 있는 유일한 방법이었다. 라디오크로믹 필름(radiochromic films, RCF)을 이용한 마이크로미터 단위의 선량 축적의 정량 분석이 가능성 있는 해결책으로 제시된다. 이 연구의 목적은 CRS 분광기가 GNP 의 선량 증감효과로 인한 라디오크로믹 필름의 활성 층의 선량 프로파일 변화 측정에 적합한 장치임을 입증하는 것이다.

비적층 라디오크로믹 EBT-XD 필름들에 200kVp 빔으로 0.3Gy 에서 50Gy 까지 조사하였다. 라만 스펙트럼은 방사선이 앞서 조사된 RCF 를 공촛점 라만분광기의 수직축과 평행하게 위치시켜 얻었다. C≡C 디아세틸렌 폴리머 스트레칭 밴드에 해당하는 라만 피크가 선택되었다. C≡C 밴드 높이는 디아세틸렌 단량체의 중합화로 인해 포화점까지 증가하는 것으로 입증되었다. 100 × 5 μm^2 의 ROI(region of interest)에 대해 스캔 분해능을 1 μm 로 설정했다. GNP 의 방사선량증감을 조사하기 위해 100 nm 금 박막을 증착한 또 다른 EBT-XD 필름 세트에 50 kVp 빔과 120 kVp 빔으로 0.5 Gy 를 조사하였다. RCF 활성 층의 선량은 표면에서 활성 층의 바닥까지 깊이 프로파일링을 통해 얻은 최대 피크 높이를 평균화하여 측정했다.

영상 획득의 공간 분해능은 변조 전달 함수 방법에 따라 정량화 하였다. 이 계산된 공간 분해능은 최소 측정 가능한 크기를 직접적으로 지시한다. 평가된 공간 분해능에 기초하여, GNF 로 조사된 필름에 전달된 선량을 계산했다. 선량 증가 계수(dose enhancement factor, DEF)는 금 증착 필름과 기본 필름의 각 측정 가능한 층에 대해 선량 측정값의 비교를 통해 얻었다. 또한 위에서 설명한 실험 설정에 따라 Geant4 에서 몬테카를로 시뮬레이션을 수행하여 실험 결과와 비교하였다. 시뮬레이션에서, RCF 활성층의 선량 증가는 1μm 마다 측정되었고, 그 결과 25 개의 층에 대한 데이터가 생성되었다. 마지막으로, 앞서 얻은 미시적 DEF 로부터 거시적 DEF 를 계산하였다.

거시적 DEF 영역은 RCF 의 전체 체적에 해당한다. 거시적 DEF 는 RCF 의 매 층마다 측정된 구조적 의미의 미시적 DEF 로부터 얻었다. 최종적으로 비교를 위해 필름의 거시적 DEF 는 이론적인 선량 축적 방정식을 이용하여 해석적으로 계산하여 얻었다.

실험을 통한 각 층의 미시적 DEF 는 몬테카를로 시뮬레이션 결과와 비교하였고, 거시적 DEF 는 실험 결과, 몬테카를로 시뮬레이션, 해석적 계산들과 비교하였다. 공촛점 라만분광기를 이용하여 라디오크로믹 필름 EBT-XD 는 6μm 의 공간 분해능을 얻었다. 50kVp 와 120kVp 에 대한 실험적 DEF 는 GNP 다음 첫 6μm 에서 각각 17.86, 14.68 이었으며 다음 층에서부터 감소하였다. 50kVp 빔에 대하여 거시적 DEF 는 실험적, 몬테칼로 시뮬레이션, 해석적 접근을 통해 각각 각각 6.5, 6.8, 5.1 로 계산되었다. 120kVp 에 대해서는 거시적 DEF 가 각각 5.4, 5.3, 4.9 였다.

금 나노 나노필름으로부터의 거리 측정으로 얻은 DEF 의 실험적 결과는 이전 연구 및 MC 시뮬레이션과 일관성이 있어 EBT-XD 시스템과 연계한 공촛점 라만분광기가 실현 가능한 마이크로미터 분해능 선량계임을 시사했다.

.....

주요어 : 공촛점 라만 분광계, 금 나노필름, 선량 증강, 방사선감광 필름, 마이크론 분해능의 선량분석, 방사선량증감.

학번: 2018-21685